Nano Research 2017, 10(11): 3865–3874
DOI 10.1007/s12274-017-1600-9
Research Article
ISSN 1998-0124
CN 11-5974/O4

Remarkable enhancement in failure stress and strain of penta-graphene via chemical functionalization

Yingyan Zhang[1], Qingxiang Pei[2] (✉), Zhendong Sha[3], Yongwei Zhang[2], and Huajian Gao[4] (✉)

[1] *School of Computing, Engineering and Mathematics, Western Sydney University, Penrith, NSW 2751, Australia*
[2] *Institute of High Performance Computing, A*STAR, Singapore 138632, Singapore*
[3] *International Center for Applied Mechanics, State Key Laboratory for Strength and Vibration of Mechanical Structures, Xi'an Jiaotong University, Xi'an 710049, China*
[4] *School of Engineering, Brown University, Providence, Rhode Island 02912, USA*

Received: 12 January 2017
Revised: 13 March 2017
Accepted: 19 March 2017

KEYWORDS
penta-graphene,
mechanical properties,
chemical functionalization,
molecular dynamics

ABSTRACT

Penta-graphene (PG), a newly proposed two-dimensional material composed entirely of carbon pentagons, is believed to possess much lower failure stress and strain than those of graphene. An open question is whether and how these properties can be enhanced. Herein using molecular dynamics simulations, we examine the deformation and failure processes of PG functionalized with different functional groups. We reveal that complete chemical functionalization leads to remarkable increases in the failure stress and strain of PG by up to 86.6% and 82.4%, respectively. The underlying reason for this enhancement is that the buckled pentagonal rings in pristine and partially functionalized PGs can easily transform into planar polygon rings under stretching; in contrast, complete functionalization of PG strongly stabilizes its structure and prevents such transformation, thereby significantly increasing the failure stress and strain. Our findings suggest a possible route to enhance the mechanical properties of PG for potential applications in nanocomposites and nanodevices.

1 Introduction

Graphene, a two-dimensional (2D) carbon allotrope with a hexagonal lattice structure, possesses many fascinating electronic properties [1–3] such as an exceptionally high charge carrier mobility of 2.5 × 10^5 $cm^2 \cdot V^{-1} \cdot s^{-1}$ [4], and thus has great potential to be used in next-generation electronics [5–9]. Graphene also possesses superior mechanical properties [10–13], with an intrinsic tensile strength of 130 GPa and a Young's modulus of 1.0 TPa, rendering it an ultra-strong reinforcing material for polymer-based nanocomposites [14, 15], as well as for various nanodevices [16, 17].

Since graphene has no bandgap, chemical functionalization, in particular hydrogenation, has been widely employed to open a bandgap and tune its electronic properties [18–25]. Hydrogenated graphene with 100% functionalization has been shown to possess

Address correspondence to Qingxiang Pei, peiqx@ihpc.a-star.edu.sg; Huajian Gao, huajian_gao@brown.edu

a bandgap as large as 3.5 eV [26]. Hydrogenation is also used to control the deformation and morphology of graphene for particular applications [27–29]. Moreover, chemical functionalization of graphene has been widely used to improve the mechanical performance of graphene/polymer nanocomposites [30, 31]. For example, by adding functional groups such as epoxide (–O–) and hydroxyl (–OH) groups on its basal plane, graphene becomes hydrophilic, and thus can be dispersed well into a polymer matrix and form strong interfacial interactions with the surrounding matrix. Consequently, the high strength and rigidity of graphene can be utilized to obtain advanced graphene-based nanocomposites with improved overall properties.

On the other hand, chemical functionalization of graphene is often accompanied with a significant deterioration in its intrinsic mechanical properties. Using atomistic simulations, it has been reported that the Young's modulus, failure strength, and strain of graphene reduced drastically with increasing hydrogen functionalization [32–34]. The fully hydrogenated graphene showed 65% reduction in the failure strength as compared to that of pristine graphene [32]. Both simulations and experiments showed that graphene oxide, an oxidized form of graphene functionalized with oxygen-containing groups, has a much lower Young's modulus and tensile strength than those of pristine graphene [35–38].

Recently, a new 2D carbon allotrope, composed entirely of carbon pentagons and resembling a Cairo-pentagonal tiling pattern, called penta-graphene (PG) has been theoretically proposed [39]. PG has a regular local buckled geometry containing sp^2- and sp^3-hybridized carbon atoms. It was predicted that PG is thermodynamically and mechanically stable, and can withstand high temperatures up to 1,000 K. PG, with an assumed wall thickness of 4.8 Å, has a high tensile strength of 40 GPa [39] and a relatively high thermal conductivity of 350 $W \cdot m^{-1} \cdot K^{-1}$ [40]. In spite of the higher tensile strength (130 GPa) and higher thermal conductivity (3,590 $W \cdot m^{-1} \cdot K^{-1}$) [40] of graphene, it has a zero band gap. PG, however, possesses an intrinsic quasi-direct bandgap as large as 3.25 eV [39, 41]. Clearly, these remarkable properties make PG a suitable candidate for applications in nanoelectronics and optoelectronics, as well as in mechanical and thermal applications of nanodevices and nanocomposites. Very recently, Xia et al. [42] reported the growth of oriented large-area pentagonal single-crystal graphene domains on Cu foils by chemical vapor deposition (CVD), which is a big step toward the experimental fabrication of PG.

Similar to graphene, chemical functionalization of PG may create opportunities to broaden its potential applications. The question then arises: How does chemical functionalization affect the mechanical properties of PG? A recent study into the thermal transport properties [40] of PG showed that its complete hydrogenation results in an unexpected 76% increase in thermal conductivity, which is in strong contrast to the 65% reduction for graphene [43]. This counterintuitive thermal conductivity enhancement in hydrogenated PG is thus the motivation to further explore the mechanical properties of chemically functionalized PG. Clearly, if functionalization can improve the mechanical properties of PG, it might introduce new ways to substitute graphene in nanocomposites and nanodevices.

In this work, we investigate the mechanical properties of PG and chemically functionalized PG using molecular dynamics (MD) simulations. In addition to hydrogenation, the influences of other functional groups such as –O– and –OH groups are explored to reveal the best functional groups for modulating the mechanical properties of PG. We find that complete hydrogenation of PG can significantly increase its failure stress and strain by 74.9% and 52.8%, respectively. This enhancement in the mechanical properties persists for the temperature range of 200–600 K. Remarkably, the hydroxyl functional groups can lead to even larger enhancement in mechanical properties, with 86.6% increase in failure stress and 82.4% in failure strain, while the epoxide group increases the failure stress and strain by 49.3% and 45.2%, respectively. The failure mechanisms of pristine and functionalized PGs are also explored. Our work not only provides a fundamental understanding of the mechanical behaviour and failure mechanisms of PG, but also shows a viable way to enhance its mechanical properties by means of chemical functionalization.

2 Results and discussion

We first study the effect of hydrogenation on the mechanical properties of PG. MD simulations were performed at 300 K for the pristine and hydrogenated PGs with four different hydrogenation coverages of 25%, 50%, 75%, and 100%. The atomic configurations of pristine and hydrogenated PGs are shown in Fig. 1.

Figure 2 shows the stress-strain curves of the pristine and hydrogenated PGs under uniaxial tensile deformation at 300 K. All the stress-strain curves start from the origin, indicating that all the models are fully relaxed before the application of external tensile loading. With the increase of tensile strain, the stress increases until it reaches the maximum value, and then drops sharply, resulting in material failure. Herein, the maximum stress is defined as the failure stress and the corresponding strain is the failure strain. The calculated failure stress and strain values of pristine PG are 50.2 GPa and 0.127, respectively.

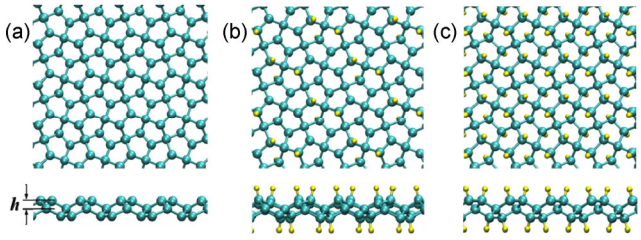

Figure 1 Atomistic configurations of (a) pristine PG, (b) 50% hydrogenated PG, and (c) 100% hydrogenated PG. Hydrogen atoms are colored in yellow; h is the out-of-plane "buckling" distance. For clarity, the top view and side view are shown in the top and bottom panels, respectively.

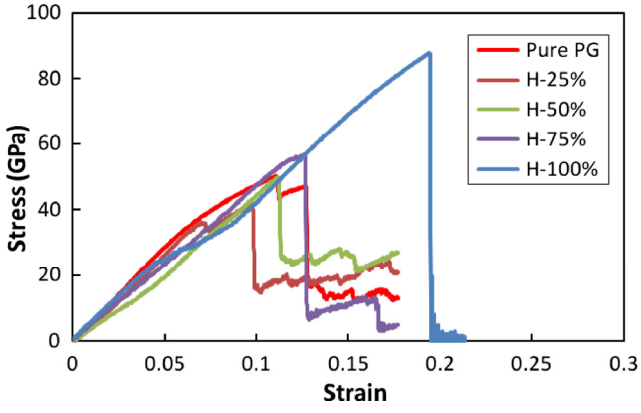

Figure 2 Stress–strain curves of pristine and hydrogenated PG at different hydrogen coverages.

These values are much lower than those of graphene as determined experimentally (130 GPa and 0.25) [10] and by MD simulations (125.2 GPa and 0.191) [44]. From Fig. 2, it is surprising to see that fully hydrogenated PG possesses the highest failure stress and strain, which means that the mechanical strength of the PG can be significantly enhanced by hydrogenation to achieve complete H-functionalization. This unexpected phenomenon is in striking contrast to graphene. When graphene is functionalized with hydrogen atoms, the transformation of planar sp^2 carbon bonds to out-of-plane sp^3 carbon bonds significantly deteriorates the mechanical properties of graphene [32, 34].

The failure stress and strain of pristine and hydrogenated PGs, as summarized in Fig. 3, exhibit an unusual down-and-up trend. When PG is hydrogenated to 25%, the failure stress and strain decrease by 16.9% and 22.8%, respectively. They then increase slightly with increasing the hydrogenation from 25% to 50%, and further to 75%. Interestingly, the failure stress and strain of the fully hydrogenated PG are enhanced by 74.9% and 52.8%, respectively, in comparison with

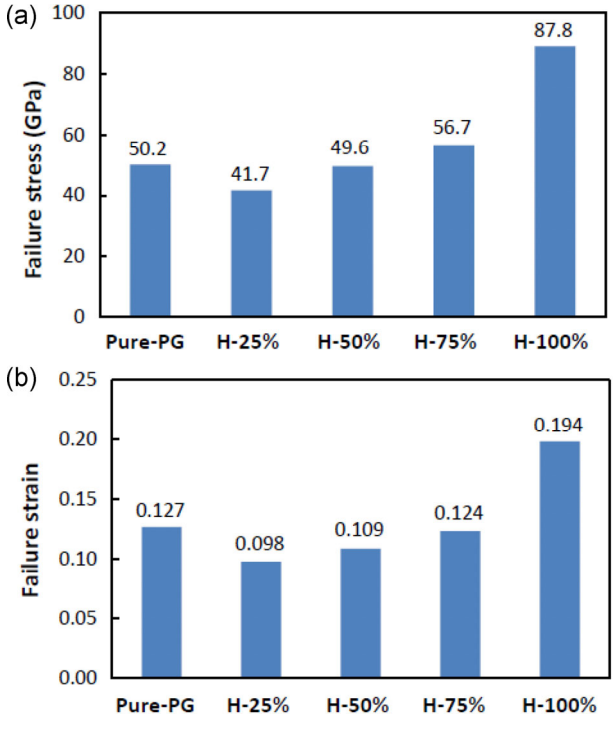

Figure 3 (a) Failure stress and (b) failure strain of pristine and hydrogenated PGs with different hydrogenation functionalities. The fully (100%) hydrogenated PG shows much higher failure stress and failure strain.

those of pristine PG. The effect of hydrogenation on the mechanical properties of PG is in strong contrast to that of hydrogenated graphene. It was shown that hydrogenation of graphene resulted in a significant reduction in its failure stress and strain [32–34]. The mechanical properties of graphene were very sensitive to hydrogenation at low functionality (< 30%) and became almost insensitive when the functionality is increased from 30% to 100% [32]. The unexpected enhancement in the mechanical properties of the fully hydrogenated PG in this study is consistent with that of its thermal conductivity [40]. Clearly, the homogenous sp^3-hydridized carbon atoms due to chemical functionalization give rise to this surprising enhancement, suggesting that fully hydrogenated PG has a weaker bond anharmonicity than pristine PG.

In order to explore the underlying mechanisms for this unexpected functionalization-induced enhancement in the mechanical properties of PG, we further examine the structure change and failure behavior of PG during tensile deformation. Snapshots of the deformation processes for pristine PG, 50% hydrogenated PG, and 100% hydrogenated PG are shown in Fig. 4. For pristine PG in Fig. 4(a), the pentagonal configuration is maintained when the tensile strain is increased from zero to 0.1251. However, when the strain is increased to 0.1273, bond breaking and structural transition occur, leading to the formation of hexagonal, heptagonal, and octagonal rings in the structure. A further increase in the strain triggers more bond breaking with the formation of more polygonal rings in the structure. This structure change indicates that pristine PG is susceptible to deformation-induced transformation from the buckled pentagonal rings to planar polygonal rings under external strain. This bond breaking and reconstruction is continuous and gradually propagates through the whole sheet with increasing strain. A similar structural transition in pristine PG was also observed in a recent MD study [45].

For hydrogenated PG, it is well known that hydrogenation changes the local C–C bonding from plane favoured sp^2 hybridization to out-of-plane favoured sp^3 hybridization. Therefore, hydrogenation helps to stabilize the local buckled structure of PG. However, for the 50% hydrogenated PG, as shown in

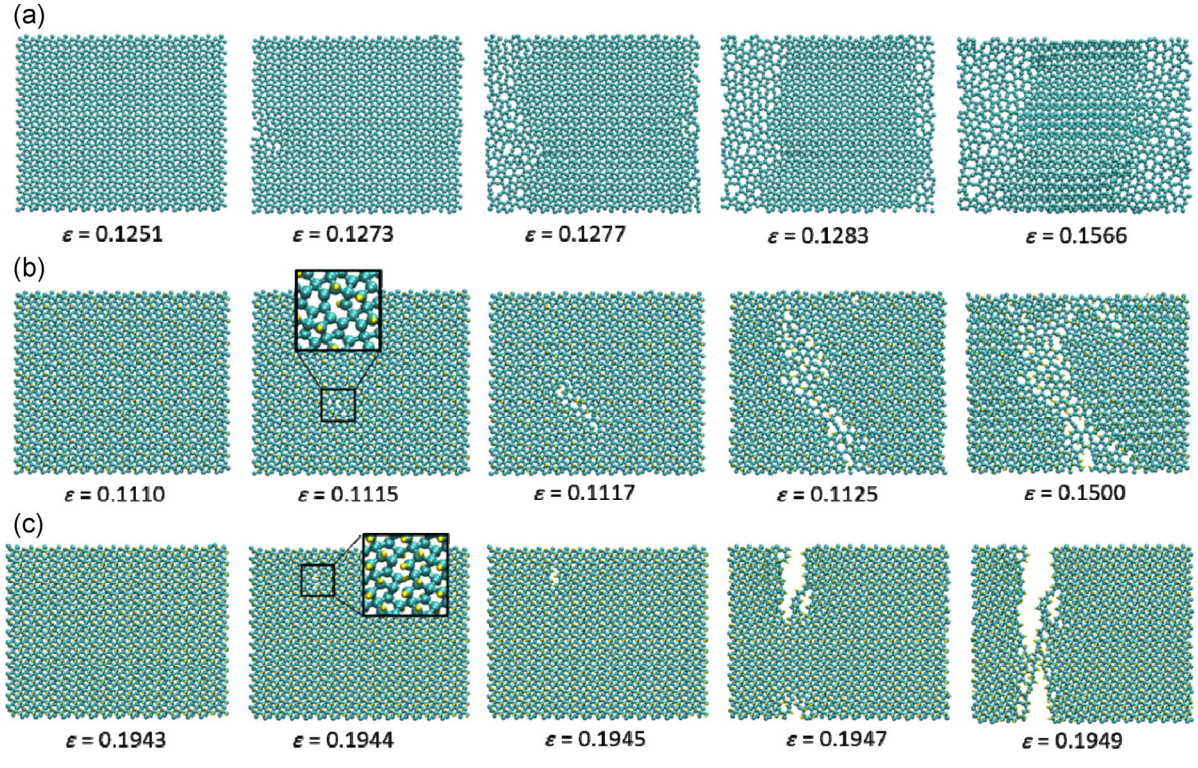

Figure 4 Snapshots of the deformation and failure processes at different uniaxial tensile strains for (a) pristine PG, (b) 50% hydrogenated PG, and (c) 100% hydrogenated PG. The insets show the locations of the initial C–C bond breaking in the structures.

Fig. 4(b), similar failure behavior as that of pristine PG is observed. The pentagonal configuration in PG is well preserved as the tensile strain is increased from zero to 0.1110. At the strain of 0.1115, bond breaking and reconstruction start, releasing the system stress. With further increase in tensile strain, more pentagonal rings transform into hexagonal, heptagonal, and octagonal rings. For the hydrogenated PG with 25% and 75% H-functionality, a similar structural transition is observed, as shown in Figs. S1 and S2 in the Electronic Supplementary Material (ESM). The similar structural change for pristine and partially hydrogenated PGs with the hydrogen functionality of 25%, 50%, and 75% explains why the failure strength and strain obtained for these PG samples are similar.

For the hydrogenated PG with 100% H-functionality, however, the failure behavior is very different, as shown in Fig. 4(c). There is no structure-transition-induced failure as observed in pristine and partially hydrogenated PGs. In the fully hydrogenated PG, all the sp^2-bonded carbon atoms become sp^3-bonded, and thus, the structural stability is greatly enhanced for the homogeneous structure. Therefore, the fully hydrogenated PG has high structural stability, which promotes its mechanical strength in resisting the external strain. It is seen in Fig. 4(c) that the 100% hydrogenated PG is able to sustain the external strain without bond breaking up to 0.1943. Initial C–C bond breaking occurs at the strain of 0.1944 and a visible crack is formed in the structure. Subsequently, the crack rapidly propagates in the direction perpendicular to the loading direction when the strain increases from 0.1945 to 0.1949, causing the fully hydrogenated PG to rupture finally.

Based on the foregoing analysis and the snapshots shown in Fig. 4, the failure mechanism of pristine and hydrogenated PGs is explained as follows: For pristine and partially hydrogenated PGs, the failure is caused by a structural transformation from 5-atom rings to 6-, 7-, 8-, or more atom rings due to the low stability of the structure. For the fully hydrogenated PG with all sp^3 hybridized bonds, the structural stability is considerably enhanced. As a result, the failure of fully hydrogenated PG occurs at much higher stress and strain levels with distinct bond-breaking and fracture stages.

In order to explore whether this significant enhancement in the mechanical properties of PG by complete hydrogenation still holds for temperatures other than 300 K, we performed MD simulations at 200, 400, 500, and 600 K for pristine and 100% hydrogenated PGs under uniaxial tensile deformation. The corresponding stress-strain curves are shown in Fig. S3 in the ESM. Figures 5(a) and 5(b) depict the failure stress and strain as a function of temperature. It can be seen that with the increase in temperature from 200 to 600 K, the failure stress and strain decrease for both pristine and fully hydrogenated PGs. The temperature-dependent failure properties can be attributed to the stronger thermal vibrations of atoms at a higher temperature, which renders the atomic bonds more likely to reach the critical bond length and then break. Despite the reduction in the mechanical properties with increasing temperature, the failure stress and strain of fully hydrogenated PG are still much higher (about 71%–88% higher) than those of pristine PG, which means that the complete-hydrogenation-induced enhancement

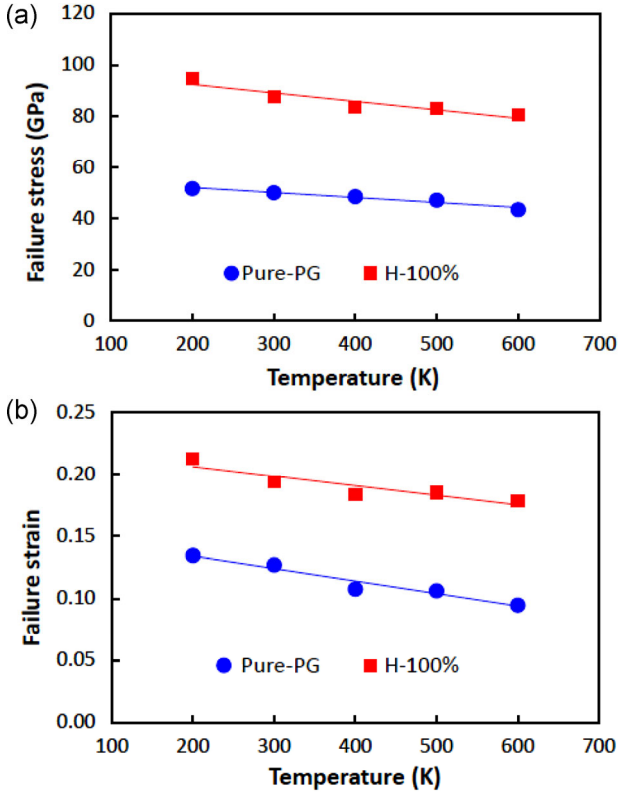

Figure 5 Effect of temperature on (a) the failure stress and (b) the failure strain of pristine PG and fully hydrogenated PG.

in the mechanical properties persists for different temperatures ranging from 200 to 600 K.

In addition to hydrogenation, other functional groups such as –O– and –OH groups are also investigated to explore whether they exert similar enhancement effects on the mechanical properties of PG. The atomic configurations of fully functionalized PG with epoxide and hydroxyl groups are shown in Fig. S4 in the ESM. Unlike the hydrogen and hydroxyl groups, which form C–H or C–O bonds with one sp^2 carbon atom in PG, the oxygen atom in the oxidized PG is bonded to two sp^2 carbon atoms as seen in Fig. S4(a) in the ESM. The stress-strain curves of fully functionalized PG with –O– and –OH groups are shown in Fig. 6(a), in which the stress-strain curves of pristine and fully hydrogenated PGs are also plotted for easy and direct comparison. It is readily seen that all of the fully functionalized PG structures outperform the pristine PG in terms of failure stress and strain. Among the three different functional groups, the fully functionalized PG with hydroxyl groups possesses the highest failure stress and strain, followed by the hydrogen and epoxide groups (see Fig. 6(b)). The hydroxyl group increases the failure stress and strain by 86.6% and 82.4%, respectively, as compared to that of the pristine PG. The epoxide group increases the failure stress and strain by 49.3% and 45.2%, respectively, while hydrogenation increases the failure stress and strain by 74.9% and 52.8%, respectively.

The snapshots of the deformation and failure processes of the PGs fully functionalized with epoxide and hydroxyl groups are shown in Fig. 7. For the PG

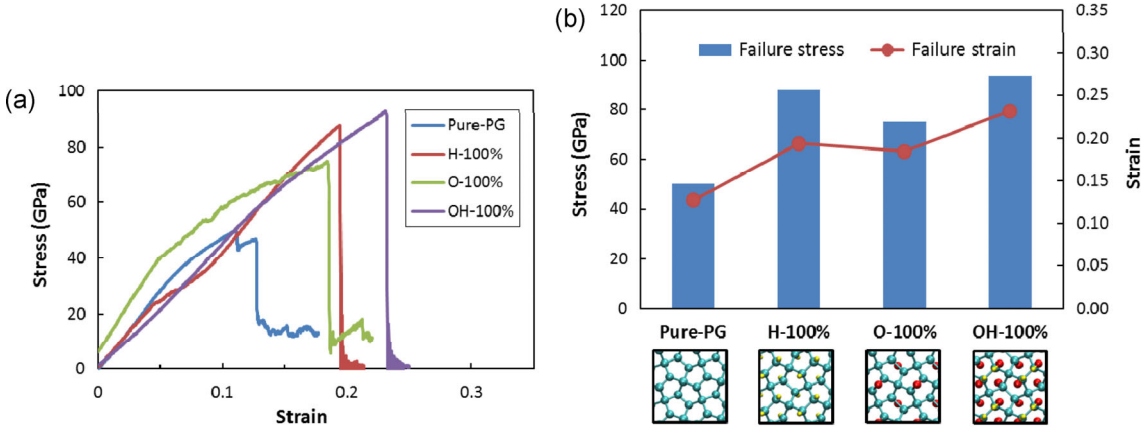

Figure 6 (a) Stress-strain curves of pristine and fully functionalized PGs with different functional groups. (b) Failure stress and failure strain of pristine and fully functionalized PGs with different functional groups.

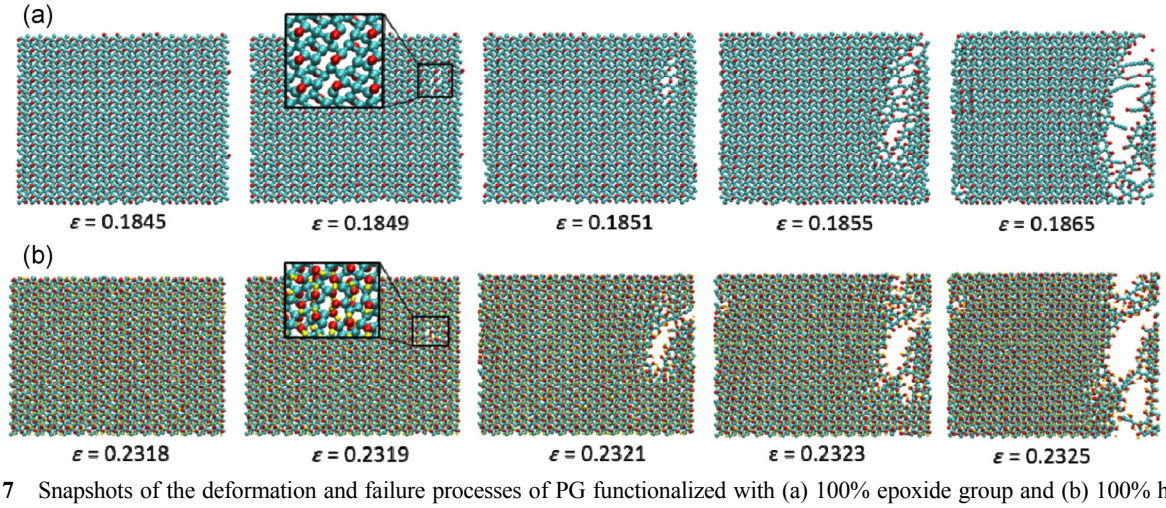

Figure 7 Snapshots of the deformation and failure processes of PG functionalized with (a) 100% epoxide group and (b) 100% hydroxyl group. The insets show the locations of initial C–C bond breaking in the structures. The oxygen and hydrogen atoms are colored in red and yellow, respectively.

functionalized with an epoxide group, it is seen from Fig. 7(a) that the structure remains stable at a relatively large strain of 0.1849. At the strain of 0.1849, initial bond breaking appears in the sp^3 C–C bonds, which connect the epoxide group. Upon further loading, the crack quickly spreads perpendicularly to the loading direction, leading to the complete failure of the structure. The failure behavior is very different from that of pristine PG shown in Fig. 4(a). Similar failure behavior is also observed for the PG functionalized with a hydroxyl group, as shown in Fig. 7(b).

In comparison with hydrogenation and hydroxylation, epoxidation is the least efficient functionalization in enhancing the failure stress and strain of PG. This is because each epoxide group is bonded to two carbon atoms in PG, distorting the local sp^3 bonds, as evidenced by the non-zero initial stress in the stress-strain curve of epoxide-functionalized PG in Fig. 6(a). The distortion in sp^3 bonds could reduce the bond stability, and therefore, the PG functionalized with epoxide groups has lower failure stress and strain than that of PG functionalized with hydrogen or hydroxyl groups.

3 Conclusions

We have investigated the effect of chemical functionalization on the mechanical properties of PG using MD simulations. Our simulation results of pristine and hydrogenated PGs with different hydrogen show that complete hydrogenation (100% coverage) significantly enhance the failure stress and strain by 74.9% and 52.8%, respectively. This enhancement in the mechanical properties of PG by complete hydrogenation persists for a broad temperature range from 200 to 600 K. The other functional groups, epoxide and hydroxyl groups, show a similar effect in enhancing the failure stress and strain, with an increase of the failure stress and strain by up to 86.6% and 82.4%, respectively. The mechanisms for this surprising increase of mechanical properties of PG induced by chemical functionalization lie in the associated structural stability. The buckled pentagonal structure in pristine PG has a higher potential energy, and thus, it is easy to convert to lower-energy structures. Complete functionalization stabilizes the PG structure by transforming all the sp^2 carbon atoms into sp^3 carbon atoms, thereby causing significant enhancement in the failure stress and strain. Our findings may have important implications for the potential applications of PG in nanocomposites and nanodevices.

4 Methods

Figure 1 shows the atomic configurations of pristine and hydrogenated PGs. The PG lattice exhibits a small buckling thickness (h) in the out-of-plane direction, in contrast to the planar structure of graphene. Due to the out-of-plane buckling, our calculations showed that PG has a potential energy of –7.57 eV·atom^{-1}, which is 2.48 eV·atom^{-1} higher than that of graphene (–10.05 eV·atom^{-1}). We showed in our MD simulations that this energy difference makes PG vulnerable to strain-induced transformation to form planar polygonal rings. A unit cell of pristine PG contains four sp^2- and two sp^3-hybridized carbon atoms. In the hydrogenated PG, hydrogen atoms are bonded to sp^2 carbon atoms only (Figs. 1(b) and 1(c)). In the case of complete hydrogenation, all the sp^2 bonds are transformed into sp^3 bonds (Fig. 1(c)). The functionalization degree (or coverage) is defined as the ratio of the number of functionalized sp^2 carbon atoms over the total number of sp^2 carbon atoms.

Our MD simulations were performed using the software package LAMMPS [46]. The interatomic interactions were described by the ReaxFF potential parameterized by Chenoweth [47] for a carbon/hydrogen/oxygen system. ReaxFF is a bond-order-dependent potential that allows for fully reactive atomistic simulations of chemical reactions, including bond breaking and rearrangement. It has been proved to accurately characterize the chemical and mechanical behaviors of hydrocarbons, diamond, graphene, carbon nanotubes, and other carbon nanostructures [48–50]. The ReaxFF produces a stable structure of PG with a buckling distance of h = 0.51 Å at room temperature (300 K), and h = 0.66 Å at 0 K, which is in good agreement with the first-principles calculations [39].

All the simulation models had in-plane dimensions of about 50 Å × 50 Å. Periodic boundary conditions

were enforced in the two in-plane directions. Uniaxial tensile loading was applied along one of the in-plane directions at a constant strain rate of 0.0005 ps^{-1} with a timestep of 0.5 fs. We tested that PG is isotropic in the in-plane directions. Prior to loading, the initial configuration was optimized by using the conjugate gradient method and then the system was relaxed fully in an NPT (constant atom number, pressure, and temperature) ensemble. During the deformation, the stresses in the system were calculated based on the atomic virial stress [51]. The atomic volume of each carbon atom was calculated from the initial relaxed PG sheet with the thickness assumed to be 4.8 Å [52]. The obtained atomic volume was used for calculating the viral stress of carbon atoms in both pristine and functionalized PGs. The stress in the stress-stain curve was computed by taking the average of all the carbon atoms in the sheet.

Acknowledgements

The authors gratefully acknowledge the computational support provided by Intersect Australia Ltd and A*STAR Computational Resource Centre of Singapore. This work was partially supported by a grant from the Science and Engineering Research Council, A*STAR, Singapore (152-70-00017). H. J. G. acknowledges support from the National Science Foundation (No. CMMI-1634492).

Electronic Supplementary Material: Supplementary material (detailed simulation methods; deformation and failure processes of 25% and 75% hydrogenated PGs; stress-strain curves of pristine and 100%-hydrogenated PGs at different temperatures; atomic configurations of PG functionalized with epoxide and hydroxyl groups) is available in the online version of this article at https://doi.org/10.1007/s12274-017-1600-9.

References

[1] Novoselov, K. S.; Geim, A. K.; Morozov, S. V.; Jiang, D.; Zhang, Y.; Dubonos, S. V.; Grigorieva, I. V.; Firsov, A. A. Electric field effect in atomically thin carbon films. *Science* **2004**, *306*, 666–669.

[2] Castro Neto, A. H.; Guinea, F.; Peres, N. M. R.; Novoselov, K. S.; Geim, A. K. The electronic properties of graphene. *Rev. Mod. Phys.* **2009**, *81*, 109–162.

[3] Morozov, S. V.; Novoselov, K. S.; Katsnelson, M. I.; Schedin, F.; Elias, D. C.; Jaszczak, J. A.; Geim, A. K. Giant intrinsic carrier mobilities in graphene and its bilayer. *Phys. Rev. Lett.* **2008**, *100*, 016602.

[4] Novoselov, K. S.; Fal'ko, V. I.; Colombo, L.; Gellert, P. R.; Schwab, M. G.; Kim, K. A roadmap for graphene. *Nature* **2012**, *490*, 192–200.

[5] Schwierz, F. Graphene transistors. *Nat. Nanotechnol.* **2010**, *5*, 487–496.

[6] Wu, Y. Q.; Jenkins, K. A.; Valdes-Garcia, A.; Farmer, D. B.; Zhu, Y.; Bol, A. A.; Dimitrakopoulos, C.; Zhu, W. J.; Xia, F. N.; Avouris, P. et al. State-of-the-art graphene high-frequency electronics. *Nano Lett.* **2012**, *12*, 3062–3067.

[7] Park, J. U.; Nam, S.; Lee, M. S.; Lieber, C. M. Synthesis of monolithic graphene-graphite integrated electronics. *Nat. Mater.* **2012**, *11*, 120–125.

[8] Das, T.; Jang, H.; Lee, J. B.; Chu, H.; Kim, S. D.; Ahn, J. H. Vertical field effect tunneling transistor based on graphene-ultrathin Si nanomembrane heterostructures. *2D Mater.* **2015**, *2*, 044006.

[9] Avouris, P.; Xia, F. N. Graphene applications in electronics and photonics. *MRS Bull.* **2012**, *37*, 1225–1234.

[10] Lee, C.; Wei, X. D.; Kysar, J. W.; Hone, J. Measurement of the elastic properties and intrinsic strength of monolayer graphene. *Science* **2008**, *321*, 385–388.

[11] Lee, G. H.; Cooper, R. C.; An, S. J.; Lee, S.; van der Zande, A.; Petrone, N.; Hammerherg, A. G.; Lee, C.; Crawford, B.; Oliver, W. et al. High-strength chemical-vapor deposited graphene and grain boundaries. *Science* **2013**, *340*, 1073–1076.

[12] Grantab, R.; Shenoy, V. B.; Ruoff, R. S. Anomalous strength characteristics of tilt grain boundaries in graphene. *Science* **2010**, *330*, 946–948.

[13] Wei, Y. J.; Wu, J. T.; Yin, H. Q.; Shi, X. H.; Yang, R. G.; Dresselhaus, M. The nature of strength enhancement and weakening by pentagon–heptagon defects in graphene. *Nat. Mater.* **2012**, *11*, 759–763.

[14] Kuilla, T.; Bhadra, S.; Yao, D. H.; Kim, N. H.; Bose, S.; Lee, J. H. Recent advances in graphene based polymer composites. *Prog. Polym. Sci.* **2010**, *35*, 1350–1375.

[15] Rafiee, M. A.; Rafiee, J.; Wang, Z.; Song, H. H.; Yu, Z. Z.; Koratkar, N. Enhanced mechanical properties of nano-composites at low graphene content. *ACS Nano* **2009**, *3*, 3884–3890.

[16] Bunch, J. S.; van der Zande, A. M.; Verbridge, S. S.; Frank, I. W.; Tanenbaum, D. M.; Parpia, J. M.; Craighead, H. G.;

McEuen, P. L. Electromechanical resonators from graphene sheets. *Science* **2007**, *315*, 490–493.

[17] Koenig, S. P.; Wang, L. D.; Pellegrino, J.; Bunch, J. S. Selective molecular sieving through porous graphene. *Nat. Nanotechnol.* **2012**, *7*, 728–732.

[18] Boukhvalov, D. W.; Katsnelson, M. I. Chemical functionalization of graphene with defects. *Nano Lett.* **2008**, *8*, 4373–4379.

[19] Boukhvalov, D. W.; Katsnelson, M. I. Chemical functionalization of graphene. *J. Phys.: Condens. Matter* **2009**, *21*, 344205.

[20] Castellanos-Gomez, A.; Wojtaszek, M.; Arramel; Tombros, N.; van Wees, B. J. Reversible hydrogenation and bandgap opening of graphene and graphite surfaces probed by scanning tunneling spectroscopy. *Small* **2012**, *8*, 1607–1613.

[21] Ryu, S.; Han, M. Y.; Maultzsch, J.; Heinz, T. F.; Kim, P.; Steigerwald, M. L.; Brus, L. E. Reversible basal plane hydrogenation of graphene. *Nano Lett.* **2008**, *8*, 4597–4602.

[22] Johns, J. E.; Hersam, M. C. Atomic covalent functionalization of graphene. *Acc. Chem. Res.* **2013**, *46*, 77–86.

[23] Tang, Q.; Zhou, Z.; Chen, Z. F. Graphene-related nanomaterials: Tuning properties by functionalization. *Nanoscale* **2013**, *5*, 4541–4583.

[24] Lonkar, S. P.; Deshmukh, Y. S.; Abdala, A. A. Recent advances in chemical modifications of graphene. *Nano Res.* **2015**, *8*, 1039–1074.

[25] Marsden, A. J.; Brommer, P.; Mudd, J. J.; Dyson, M. A.; Cook, R.; Asensio, M.; Avila, J.; Levy, A.; Sloan, J.; Quigley, D. et al. Effect of oxygen and nitrogen functionalization on the physical and electronic structure of graphene. *Nano Res.* **2015**, *8*, 2620–2635.

[26] Sofo, J. O.; Chaudhari, A. S.; Barber, G. D. Graphane: A two-dimensional hydrocarbon. *Phys. Rev. B* **2007**, *75*, 153401.

[27] Zhu, S. Z.; Li, T. Hydrogenation-assisted graphene origami and its application in programmable molecular mass uptake, storage, and release. *ACS Nano* **2014**, *8*, 2864–2872.

[28] Zhang, Z. Q.; Liu, B.; Hwang, K. C.; Gao, H. J. Surface-adsorption-induced bending behaviors of graphene nanoribbons. *Appl. Phys. Lett.* **2011**, *98*, 121909.

[29] Liu, B.; Baimova, J. A.; Dmitriev, S. V.; Wang, X.; Zhu, H. W.; Zhou, K. Discrete breathers in hydrogenated graphene. *J. Phys. D: Appl. Phys.* **2013**, *46*, 305302.

[30] Kuila, T.; Bose, S.; Mishra, A. K.; Khanra, P.; Kim, N. H.; Lee, J. H. Chemical functionalization of graphene and its applications. *Prog. Mater. Sci.* **2012**, *57*, 1061–1105.

[31] Wang, Y.; Yang, C. H.; Cheng, Y.; Zhang, Y. Y. A molecular dynamics study on thermal and mechanical properties of graphene-paraffin nanocomposites. *RSC Adv.* **2015**, *5*, 82638–82644.

[32] Pei, Q. X.; Zhang, Y. W.; Shenoy, V. B. A molecular dynamics study of the mechanical properties of hydrogen functionalized graphene. *Carbon* **2010**, *48*, 898–904.

[33] Popova, N. A.; Sheka, E. F. Mechanochemical reaction in graphane under uniaxial tension. *J. Phys. Chem. C* **2011**, *115*, 23745–23754.

[34] Peng, Q.; Liang, C.; Ji, W.; De, S. A theoretical analysis of the effect of the hydrogenation of graphene to graphane on its mechanical properties. *Phys. Chem. Chem. Phys.* **2013**, *15*, 2003–2011.

[35] Liu, L. Z.; Zhang, J. F.; Zhao, J. J.; Liu, F. Mechanical properties of graphene oxides. *Nanoscale* **2012**, *4*, 5910–5916.

[36] Suk, J. W.; Piner, R. D.; An, J.; Ruoff, R. S. Mechanical properties of monolayer graphene oxide. *ACS Nano* **2010**, *4*, 6557–6564.

[37] Dikin, D. A.; Stankovich, S.; Zimney, E. J.; Piner, R. D.; Dommett, G. H. B.; Evmenenko, G.; Nguyen, S. T.; Ruoff, R. S. Preparation and characterization of graphene oxide paper. *Nature* **2007**, *448*, 457–460.

[38] Liu, Y. L.; Xie, B.; Zhang, Z.; Zheng, Q. S.; Xu, Z. P. Mechanical properties of graphene papers. *J. Mech. Phys. Solids* **2012**, *60*, 591–605.

[39] Zhang, S. H.; Zhou, J.; Wang, Q.; Chen, X. S.; Kawazoe, Y.; Jena, P. Penta-graphene: A new carbon allotrope. *Proc. Natl. Acad. Sci. USA* **2015**, *112*, 2372–2377.

[40] Wu, X. F.; Varshney, V.; Lee, J.; Zhang, T.; Wohlwend, J. L.; Roy, A. K.; Luo, T. F. Hydrogenation of penta-graphene leads to unexpected large improvement in thermal conductivity. *Nano Lett.* **2016**, *16*, 3925–3935.

[41] Yu, Z. G.; Zhang, Y. W. A comparative density functional study on electrical properties of layered penta-graphene. *J. Appl. Phys.* **2015**, *118*, 165706.

[42] Xia, K. L.; Artyukhov, V. I.; Sun, L. F.; Zheng, J. Y.; Jiao, L. Y.; Yakobson, B. I.; Zhang, Y. Y. Growth of large-area aligned pentagonal graphene domains on high-index copper surfaces. *Nano Res.* **2016**, *9*, 2182–2189.

[43] Pei, Q. X.; Sha, Z. D.; Zhang, Y. W. A theoretical analysis of the thermal conductivity of hydrogenated graphene. *Carbon* **2011**, *49*, 4752–4759.

[44] Zhang, Y. Y.; Pei, Q. X.; Wang, C. M. Mechanical properties of graphynes under tension: A molecular dynamics study. *Appl. Phys. Lett.* **2012**, *101*, 081909.

[45] Cranford, S. W. When is 6 less than 5? Penta- to hexa-graphene transition. *Carbon* **2016**, *96*, 421–428.

[46] Plimpton, S. Fast parallel algorithms for short-range molecular dynamics. *J. Comput. Phys.* **1995**, *117*, 1–19.

[47] Chenoweth, K.; van Duin, A. C. T.; Goddard, W. A., III. ReaxFF reactive force field for molecular dynamics simulations

of hydrocarbon oxidation. *J. Phys. Chem. A* **2008**, *112*, 1040–1053.

[48] Jensen, B. D.; Wise, K. E.; Odegard, G. M. Simulation of the elastic and ultimate tensile properties of diamond, graphene, carbon nanotubes, and amorphous carbon using a revised ReaxFF parametrization. *J. Phys. Chem. A* **2015**, *119*, 9710–9721.

[49] Cranford, S. W.; Buehler, M. J. Mechanical properties of graphyne. *Carbon* **2011**, *49*, 4111–4121.

[50] Nielson, K. D.; van Duin, A. C. T.; Oxgaard, J.; Deng, W. Q.; Goddard, W. A., III. Development of the ReaxFF reactive force field for describing transition metal catalyzed reactions, with application to the initial stages of the catalytic formation of carbon nanotubes. *J. Phys. Chem. A* **2005**, *109*, 493–499.

[51] Diao, J. K.; Gall, K.; Dunn, M. L. Atomistic simulation of the structure and elastic properties of gold nanowires. *J. Mech. Phys. Solids* **2004**, *52*, 1935–1962.

[52] Xu, W.; Zhang, G.; Li, B. W. Thermal conductivity of penta-graphene from molecular dynamics study. *J. Chem. Phys.* **2015**, *143*, 154703.